Time-evolution patterns of electrons in twisted bilayer graphene

V. Nam Do,[1,*] H. Anh Le,[1] and D. Bercioux[2,3]

[1]*Phenikaa Institute for Advanced Study (PIAS), Phenikaa University, Hanoi 10000, Vietnam*

[2]*Donostia International Physics Center (DIPC), Manuel de Lardizbal 4, E-20018 San Sebastían, Spain*

[3]*IKERBASQUE, Basque Foundation of Science, 48011 Bilbao, Basque Country, Spain*

(Received 9 January 2019; revised manuscript received 26 March 2019; published 19 April 2019)

We characterize the dynamics of electrons in twisted bilayer graphene by analyzing the time evolution of electron waves in an atomic lattice. We perform simulations based on a kernel polynomial technique using Chebyshev polynomials; this method does not requires any diagonalization of the system Hamiltonian. Our simulations reveal that interlayer electronic coupling induces an exchange of waves between the two graphene layers. This wave transfer manifests as oscillations of the layer-integrated probability densities as a function of time. For the bilayer case, it also causes a difference in the wavefront dynamics compared to monolayer graphene. The intralayer spreading of electron waves is irregular and progresses as a two-stage process. The first one, characterized by a well-defined wavefront, occurs in a short time—a wavefront forms instead during the second stage. The wavefront takes a hexagonlike shape with the vertices developing faster than the edges. Though the detail spreading form of waves depends on initial states, we observe localization of waves in specific regions of the moiré zone. To characterize the electron dynamics, we also analyze the time autocorrelation functions. We show that these quantities exhibit beating modulation when reducing interlayer coupling.

DOI: 10.1103/PhysRevB.99.165127

I. INTRODUCTION

Stacking two-dimensional (2D) materials [1] is a novel method based on the *lego* principle for creating new van der Waals heterostructures with well-controlled properties [2]. However, according to the principles of this method, the successive layers are only stacked vertically, maintaining the same orientation as the layer below. An important step forward comes from allowing a change in the relative orientation of the different stacked layers. The simplest system allowing this new stacking method is twisted bilayer graphene (TBG). This system, which has been receiving a great deal of attention recently, is composed of two graphene layers stacked in a general manner [3]. It was predicted that twisting two graphene layers allows for a strong tuning of its electronic properties [4–8]. Interestingly, a very narrow isolated energy band around the charge-neutrality level may appear in the spectrum of TBG configurations with tiny twist angles [6]. Recently, Cao *et al.* have demonstrated experimentally that this narrow flat band is responsible for several strongly correlated phases, including an unconventional superconducting phase and a Mott-like phase [9,10]. Theoretically, it was shown by Zou *et al.* that there are obstructions involving the symmetries of the TBG lattice in constructing effective continuum and tight-binding models to characterize the dynamics of electrons occupying the flat band [11,12].

Generally, stacking two layered materials may result in a system of reduced symmetry compared to the two constituent lattices. The atomic configurations of TBG can be characterized by an in-plane vector $\boldsymbol{\tau}$ and a twist angle θ defining, respectively, the relative shift and rotation between the two graphene lattices. However, it is shown that only the twist angle governs the commensurability of the stacking, regardless of the twisting center [5,11,13,14]. In particular, the lattice alignment is commensurate only when the twist angle takes the values given by the formula $\theta = \text{acos}[(3m^2 + 3mr + r^2/2)/(3m^2 + 3mr + r^2)]$, in which m, r are positive coprime integers [5,11,13–16]. When the stacking is commensurate, the translational symmetry of the TBG lattice is preserved, but it usually defines a large unit cell, especially for small twist angles θ. The electronic calculation for such TBG configurations by brute force diagonalization is therefore extremely expensive in terms of computational resources [17–21]. Furthermore, the electronic calculations based on the time-independent Schrödinger/Kohn-Sham equation combined with the Bloch theorem are not applicable for incommensurate configurations because of the loss of the lattice translational invariance. In this work, we show that methods based on the time-dependent Schrödinger equation in real space are a powerful alternative to treat the TBG system of arbitrary twist angles.

Following the time evolution of wave packets in real space is a useful technique to simulate the dynamics of electrons. This method was used for studying the case of monolayer graphene and special TBG configurations. For instance, Rusin and Zawadzki [22] and Maksimova *et al.* [23] used the kicked Gaussian wave packet to analytically study the different features of the zitterbewegung motion of electrons in various carbon-based structures, including carbon nanotubes. In these works, the wave-packet dynamics was governed by an effective Dirac Hamiltonian, thus the discrete nature of the atomic lattice was not taken into account. Márk *et al.* [24], however, described the evolution of the kicked Gaussian wave packet in

*nam.dovan@phenikaa-uni.edu.vn

a potential field constructed from an atomistic pseudopotential model. This approach allows us to take into account the distortion of the Dirac cones at high energy, and thus shows the anisotropic dynamics of electrons in the graphene lattice. In a tight-binding framework, Chaves *et al.* [25] used the discrete Gaussian form to define a wave packet and showed some quantitative differences in the zitterbewegung motion of an electron described by the effective Dirac model and the tight-binding description. Xian *et al.* [26] also used the discrete Gaussian wave packet to simulate the transport of an electron in a particular commensurate TBG. They showed the existence of six preferable transport directions along which the wave packets are not broadened; these are along the direction perpendicular to the transport direction. In particular, they discussed the behavior of the layer-integrated probability density in each layer. They interpreted its behavior as similar to the neutrino-like oscillations where the interlayer coupling plays the role of mixing Dirac fermions in each layer: the two neutrino flavors.

It is well known that the honeycomb structure of graphene, as the chiral interlocking of two triangle sublattices, is responsible for all the peculiar properties of graphene and related systems. Accordingly, the electronic properties of graphene can be described using a formulation in terms of relativistic fermions [27]. This formulation is the same one used by Schrödinger to show the zitterbewegung phenomena as a result of the interference of states at positive and negative energies [28,29]. The two-component spinor structure of the low-energy electron states in graphene is due to the unit cell of the honeycomb lattice constituted by only two carbon atoms. Stacking two graphene sheets gives rise to the diversity of the TBG configurations. It is therefore natural to wonder about the manifestation of the atomic lattice structure on the dynamical behavior of electrons, particularly in the TBG systems with the lack of translational symmetry.

In this work, we address the dynamics of electrons in the real lattice of generic TBG configurations using the tight-binding approach, and we try to relate it to the lattice symmetries. Though the wave-packet method has been successfully used to demonstrate the optical analogy of electrons in graphene [30–34], its definition depends explicitly on some parameters and therefore it cannot provide a full picture of the electronic properties of a system. Accordingly, we will analyze the time evolution of localized electrons occupying the $2p_z$ orbitals of a carbon atom instead of Gaussian wave packets, whose definition depends on a particular wave vector and an initial position. Within this approach, we can study the changes in the evolution pattern of electron wave functions with respect to the details of the lattice structure. By artificially tuning the value of the parameters encoding the hybridization of the $2p_z$ orbitals between two graphene layers, we study the role of interlayer coupling on the time evolution of electron states. To study the time evolution of a state, we use the formalism of the time-evolution operator $\hat{U}(t)$, i.e., $|\psi(t)\rangle = \hat{U}(t)|\psi(0)\rangle$; we employ the kernel polynomials method to approximate $\hat{U}(t)$ [35]. This method is efficient and useful to work directly in the lattice space of TBG configurations with arbitrary twist angles. Technically, we use the Chebyshev polynomials of the first kind to approximate the operator $\hat{U}(t)$. Our implementation scheme is efficient because it accounts for the recursive relations of these polynomials, and, as a matter of fact, we are never performing a numerical diagonalization of the system Hamiltonian. Within this method, we can incorporate the details of a discrete atomic lattice into the dynamical properties of the $2p_z$ electrons of the TBGs. We shall study the intralayer development of the $2p_z$ orbitals and the transfer of the probability density from one graphene layer to the other. The local information of the dynamics is studied in the time domain.

The outline of this paper is as follows. In Sec. II, we present an empirical tight-binding model, which allows us to characterize the dynamics of the $2p_z$ electrons in different levels of hopping approximation, i.e., the nearest-neighbor (NN), next-nearest-neighbor (NNN), and next-next-nearest-neighbor (NNNN), and we also present the method for the investigation of the time evolution of the states as well as the calculation for several physical quantities characterizing the dynamics of electrons. In Sec. III, we present results for various graphene systems: single-layer graphene, TBG in the AA and AB configuration, and finally for various TBGs with generic twist angles. Finally, we present conclusions in Sec. IV.

II. CALCULATION METHOD

In this section, we present the empirical method for defining the tight-binding Hamiltonian for TBG. Subsequently, we present the method for evaluating the time evolution of a state, and the calculation of the probability density and the density of the probability current based on the kernel polynomial method [35]. Furthermore, we present also a method for evaluating the time autocorrelation function involving the time evolution of a state. This quantity provides insight into the electronic structure of the system under study.

A. The empirical tight-binding Hamiltonian

The Hamiltonian defining the dynamics of the $2p_z$ electrons reads [36]

$$\mathcal{H}_{\mathrm{TBG}} = \sum_{\nu=1}^{2}\left[\sum_{i,j} t_{ij}^{\nu}\hat{c}_{\nu i}^{\dagger}\hat{c}_{\nu j} + \sum_{i} V_i^{\nu}\hat{c}_{\nu i}^{\dagger}\hat{c}_{\nu i}\right] + \sum_{\nu=1}^{2}\sum_{ij} t_{ij}^{\nu\bar{\nu}}\hat{c}_{\nu i}^{\dagger}\hat{c}_{\bar{\nu} j}. \quad (1)$$

In this Hamiltonian, the terms in the square brackets define the hopping of the $2p_z$ electron in two graphene monolayers (the index ν denotes the layer), with t_{ij}^{ν} the intralayer hopping energies between two lattice nodes i and j, and V_i^{ν} the on-site energies that are generally introduced to include local spatial effects. The creation and annihilation of an electron at a layer "ν" and a lattice node "i" are encoded by the operators $\hat{c}_{\nu i}^{\dagger}$ and $\hat{c}_{\nu i}$, respectively. The hopping of an electron between two layers is described by the last term of the Hamiltonian characterized by the hopping parameters $t_{ij}^{\nu\bar{\nu}}$. The notation $\bar{\nu}$ implies that $\bar{\nu} \neq \nu$. The values of the hopping parameters t_{ij}^{ν}

and $t_{ij}^{\nu\bar{\nu}}$ are obtained via the model [37,38]

$$t_{ij} = V_{pp\pi}^0 \exp\left(-\frac{R_{ij}-a_{cc}}{r_0}\right)\left[1-\left(\frac{\mathbf{R}_{ij}\cdot\mathbf{e}_z}{R_{ij}}\right)^2\right] + V_{pp\sigma}^0 \exp\left(-\frac{R_{ij}-d}{r_0}\right)\left(\frac{\mathbf{R}_{ij}\cdot\mathbf{e}_z}{R_{ij}}\right)^2. \quad (2)$$

This model for the hopping parameters is constructed through two Slater-Koster parameters $V_{pp\pi} \approx -2.7$ eV and $V_{pp\sigma} \approx 0.48$ eV. These parameters characterize the hybridization of the nearest-neighbor $2p_z$ orbitals in the intralayer and interlayer graphene sheets, respectively. The hopping parameters decay with exponential law as a function of the distance between the lattice nodes $R_{ij} = |\mathbf{R}_{ij}|$; $\mathbf{R}_{ij}$ is the vector connecting two lattice sites i and j, $\mathbf{e}_z$ is the unit vector along the z-direction perpendicular to the two graphene layers, and $d \approx 0.335$ nm is the distance between two graphene layers. Accordingly, when i and j belong to the same layer, $\mathbf{R}_{ij}$ is perpendicular to $\mathbf{e}_z$ so that we obtain the intralayer hopping $t_{ij}^{\nu} = V_{pp\pi}\exp[-(R_{ij}-a_{cc})/r_0]$, otherwise we get $t_{ij}^{\nu\bar{\nu}}$. The other parameters are defined as $r_0 \approx 0.184\sqrt{3}a_{cc}$, an empirical parameter characterizing the decay of the electron hopping, and $a_{cc} \approx 1.42$ Å, the distance between two nearest carbon atoms in the graphene lattice. In this work, we are interested in the intrinsic properties of TBG, so we simply set the on-site energies V_i^{σ} to be zero.

B. The formalisms for the time evolution of a state

Let us start by considering an initial state $|\psi(0)\rangle$ at the time $t = 0$. This state can evolve in time to $|\psi(t)\rangle$ by acting on it with the time-evolution operator $\hat{U}(t) = \exp(-i\hat{H}t/\hbar)$:

$$|\psi(t)\rangle = \hat{U}(t)|\psi(0)\rangle = \exp(-i\hat{H}t/\hbar)|\psi(0)\rangle. \quad (3)$$

This equation is the formal solution of the time-dependent Schrödinger equation, where $\hat{H}$ denotes the Hamiltonian operator. We account for the discrete nature of the atomic lattice by describing the system within a tight-binding approximation presented in the Sec. II A.

In writing the tight-binding Hamiltonian (1), we use a localized basis set $\{|j\rangle, j = 1,\ldots,N\}$ to specify the representation. Here, ket $|j\rangle$ denotes the $2p_z$ orbital located at the lattice node j, and N is the total number of lattice nodes of the whole system. We can express a state $|\psi(t)\rangle$ in this basis set in the following way:

$$|\psi(t)\rangle = \sum_{j=1}^{N} g_j(t)|j\rangle, \quad (4)$$

where $g_j(t)$ determines the probability amplitude of finding an electron at node j at time t. The probability density $P_j(t) = |\langle j|\psi(t)\rangle|^2 = |g_j(t)|^2$ is the quantity determining the dynamics of the electron states. The value of $g_j(t)$ is obtained by solving the time-dependent Schrödinger equation or equivalently by performing the calculation for Eq. (3).

In this work, we evaluate the time-evolution operator $\hat{U}(t)$ by expanding it in terms of the Chebyshev polynomials of the first kind, $Q_m(x) = \cos[m\arccos(x)]$ [35]. As first, we rescale the spectrum of the Hamiltonian $\hat{H}$ to the interval $[-1, 1]$. This scaling is obtained by replacing $\hat{H} = W\hat{h} + E_0$, wherein W is half of the spectrum bandwidth, E_0 is the central point of the spectrum, and $\hat{h}$ is the rescaled Hamiltonian. Practically, we use the power method to estimate W. The time-evolution operator is therefore expanded regarding the Chebyshev polynomials as follows:

$$\hat{U}(t) = e^{iE_0t/\hbar}\sum_{m=0}^{+\infty}\frac{2}{\delta_{m,0}+1}(-i)^m B_m\left(\frac{Wt}{\hbar}\right)Q_m(\hat{h}), \quad (5)$$

where B_m is the m-order Bessel function of the first kind, and $\delta_{m,0}$ is the Kronecker symbol. We define the so-called Chebyshev vectors $|\phi_m\rangle = Q_m(\hat{h})|\psi(0)\rangle$, which can be calculated using the recursive relation

$$|\phi_m\rangle = 2\hat{h}|\phi_{m-1}\rangle - |\phi_{m-2}\rangle, \quad (6)$$

with $|\phi_0\rangle = |\psi(0)\rangle$ and $|\phi_1\rangle = \hat{h}|\phi_0\rangle$. Thus, the state $|\psi(t)\rangle$ is formally obtained via

$$|\psi(t)\rangle = e^{iE_0t/\hbar}\sum_{m=0}^{+\infty}\frac{2}{\delta_{m,0}+1}(-i)^m B_m\left(\frac{Wt}{\hbar}\right)|\phi_m\rangle. \quad (7)$$

This equation is exact, but we cannot numerically perform the summation of an infinite series. We therefore approximate $|\psi(t)\rangle$ by a finite series of M terms. Unfortunately, this truncation breaks the preservation of the norm of $|\psi(t)\rangle$. Practically, the number of terms M contributing to the summation in Eq. (7) is chosen to guarantee the norm conservation of $|\psi(t)\rangle$ in a finite, but sufficiently long, evolution time. For instance, in order to evolve a state in a square TBG sample with 100 nm size for an evolution time of 50 fs, M should be about 1200 [36].

To define the initial condition for the time-dependent Schrödinger equation, one usually assumes the wave function at $t = 0$ of a Gaussian form [39],

$$\psi_{\mathbf{k}}(\mathbf{r}, t=0) = \frac{1}{\sigma\sqrt{\pi}}\exp\left[-\frac{(\mathbf{r}-\mathbf{r}_0)^2}{2\sigma^2}\right]\phi_{\mathbf{k}_0}(\mathbf{r}).$$

In this Gaussian form, $\phi_{\mathbf{k}_0}(\mathbf{r})$ can be simply chosen as a plane wave $\exp(i\mathbf{k_0}\mathbf{r})$ or generally as a Bloch function defining a propagating electron state [26]. The Gaussian prefactor modulates the extension of the function $\phi_{\mathbf{k}_0}(\mathbf{r})$ localized around the position $\mathbf{r}_0$ with a width of σ. The advantage of this choice is that it allows simulating both the spreading and the moving of the wave centroid. However, the particular behavior of these phenomena varies concerning σ and $\mathbf{k}_0$, two parameters defining a certain initial state.

In this work, we follow a different strategy: we choose a lattice node randomly, then we select the corresponding $2p_z$ orbital to be the initial state. It means that we choose the coefficients $g_j(t=0) = \delta_{ij}e^{i\phi}$, where ϕ is a random real number, and thus

$$|\psi(t=0)\rangle = \sum_{j=1}^{N}\delta_{ij}e^{i\phi}|j\rangle = e^{i\phi}|i\rangle. \quad (8)$$

While this choice does not allow us to simulate the displacement of the wave centroid, it does enable us to study the whole energy spectrum of the $2p_z$ electron through the spreading of waves in the various graphene systems.

To quantify the electron transport, we calculate the expectation value of the probability current operator. In the tight-binding description, the probability current operator reads [36]

$$\hat{\mathbf{J}} = \frac{i}{\hbar}\sum_{j,k=1}^{N}(\mathbf{r}_j - \mathbf{r}_k)t_{jk}\hat{c}_j^{\dagger}\hat{c}_k. \tag{9}$$

Its expectation value on the state $|\psi(t)\rangle$ is expressed as $\langle\hat{\mathbf{J}}\rangle(t) = \sum_{j=1}^{N}\mathbf{J}_j(t)$, where $\mathbf{J}_j(t)$ is interpreted as the density of the probability current:

$$\mathbf{J}_j(t) = -\frac{1}{\hbar}\sum_i(\mathbf{r}_j - \mathbf{r}_i)\mathrm{Im}[t_{ij}g_i^*(t)g_j(t)]. \tag{10}$$

The study of the time evolution of a state gives us information on the electronic structure of the system. Given an initial state $|\psi(0)\rangle$, the time autocorrelation function $C_\psi(t)$ is defined as the projection of $|\psi(t)\rangle$ on its initial state $|\psi(0)\rangle$:

$$C_\psi(t) = \langle\psi(0)|\psi(t)\rangle. \tag{11}$$

In the tight-binding representation with the initial states chosen as localized at a particular lattice node $|\psi(0)\rangle = |i\rangle$, the time autocorrelation $C_i(t) = \langle i|\psi(t)\rangle = g_i(t)$, i.e., it is equal to the local probability amplitude at node i. Its power spectrum, defined as the Fourier transform of $C_i(t)$, is the local density of states of an electron in the considered system [35,36],

$$\rho_i(E) = \frac{s}{\pi\hbar\Omega_a}\mathrm{Re}\left[\int_0^{+\infty} dt\, e^{iEt/\hbar}C_i(t)\right], \tag{12}$$

where Ω_a is the volume assigned for each atom in the lattice, and $s = 2$ counts the spin degeneracy. We can obtain the system's total density of states from Eq. (12) by replacing $C_i(t)$ by an ensemble average of $C_i(t)$ over a small set of initial states $|i\rangle$. We implemented this procedure for the first time in Ref. [36], and results for an extremely tiny twist configuration of TBG were in agreement with the approach of continuum models [7].

III. RESULTS AND DISCUSSION

In this section, we present results for the three mentioned physical quantities introduced in the previous section: the probability density $P_j(t)$, the density of probability current $\mathbf{J}_j(t)$, and the time autocorrelation function $C_i(t)$, to characterize the dynamics of electrons in monolayer and bilayer graphene systems.

A. Monolayer graphene

To better understand the physics of TBG, we start by analyzing the more straightforward case of monolayer graphene. We performed the calculation for the tight-binding Hamiltonians accounting for the NN, NNN, and NNNN hopping terms. As we shall see later, the three models result in different quantitative behavior for the time autocorrelation function, but they have the same spreading pattern of the electron wave function; thus for simplicity, we will present results only for the NN case.

We present in Fig. 1 the distribution of the probability densities $P_j(t) = |g_j(t)|^2$ and the probability current densities $\mathbf{J}_j(t)$ obtained for the spreading of a $2p_z$ state initially located at a single lattice node. At each lattice node, we use the solid circles and the arrows to represent the probability densities and the probability current densities, respectively. The circle radius is proportional to the value of $P_j(t)$, which is normalized at each t to the maximal value of the set $\{P_j(t)\}, \forall\ j \in \{1,\ldots,N\}$. Similarly, the arrow length is proportional to the length of $\mathbf{J}_j(t)$, which is also scaled appropriately. The length and the direction of the arrows indicate the tendency for the probability density at a lattice node to transfer to the neighbor lattice nodes.

The time frames taken at $t = 0.1$ and 0.2 fs show that the state first spreads to the three nearest neighbors oriented by the angles π and $\pm\pi/3$, i.e., along the direction of the armchair lines (highlighted in red in Fig. 1; frame with $t = 0.8$ fs). The instants $t = 0.4$ and 0.6 fs show that the probability current density tends to flow from the central point to the outside along the three directions determined by the angles 0 and $\pm 2\pi/3$, i.e., also along the direction of the armchair lines. However, at $t = 0.8$ fs the dynamic shows clearly six dominant spreading directions of the probability density, oriented along the directions of the angles $\pm\pi/6$, $\pm\pi/2$, and $\pm 5\pi/6$, i.e., along the zigzag lines of the honeycomb lattice (cf. Fig. 1; frame with $t = 0.8$ fs). For the other time frames, at $t \in [1, 2]$ fs, we find a continuous spreading of the electron wave function, and we observe the formation of a wavefront with a hexagonal shape. After 2 fs, the wavefront is well established with the corners heading the directions of the zigzag lines.

To quantify the pattern of the wave spreading, we directly inspected the distribution of both the probability densities $P_j(t)$ and the probability current densities $\mathbf{J}_j(t)$ on the lattice nodes. We learned that the distribution of these two quantities obeys the features of the point group D_{3h}. These symmetry properties are not identical to those of the graphene lattice, described by the symmorphic space group $p6mm$, and thus the point group D_{6h} [40]. However, we should remember that D_{3h} is a subgroup of D_{6h}, and is the point group of the lattice node. We then conclude that the spreading pattern of electrons depends on not only the lattice symmetry, but also the symmetry of the initial state.

To get quantitative information on the energy spectrum of the π-bands from the observation of the spreading of a $2p_z$ state, we calculated the time autocorrelation function $C_i(t)$ [cf. Eq. (11)]. The Fourier transform of $C_i(t)$ provides the local density of states at the lattice node i [36]. In our calculation, we found that the time autocorrelation function, despite being a complex function in general, gets purely real when we consider a model with only NN hopping. In Fig. 2 we show the value of $C_i(t)$ obtained by invoking the three hopping models. The result shows the oscillating behavior of $C_i(t)$ as a function of time with decreasing magnitude. This behavior implies the declining of the correlation at long evolution times. For the NN hopping approximation, the Hamiltonian has only one parameter $t_{cc} = V_{pp\pi}^0$, which sets the energy scale. In this case, we find that $C_i(t)$ is periodic with the oscillation pattern mentioned in Fig. 2. By

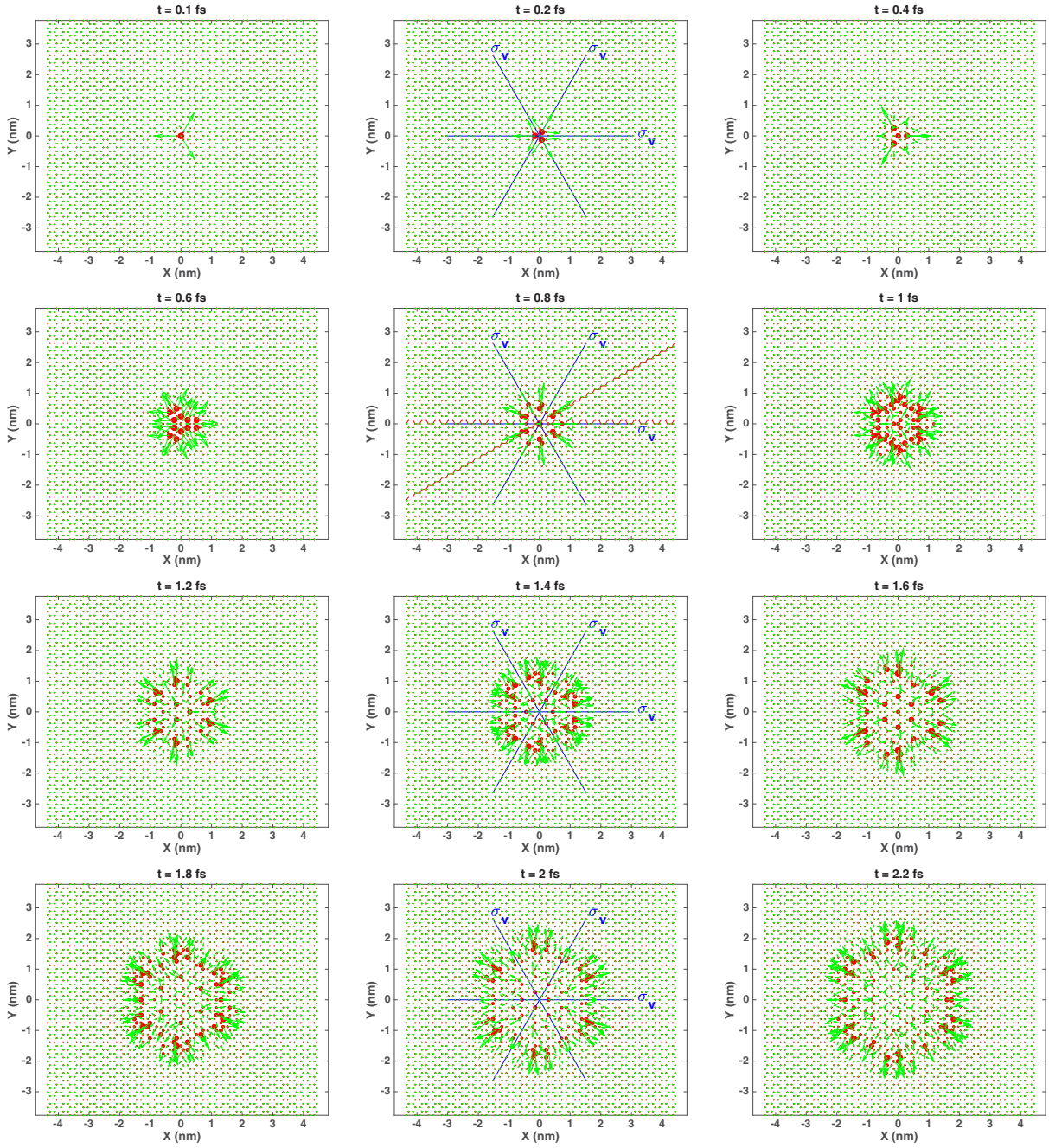

FIG. 1. Spreading of the distribution of electron probability densities (in red) in the monolayer graphene taken at several time moments. The arrows denote the vectors of probability current density (in green). The blue lines denote the three mirror-symmetry planes σ_v of the hexagonal lattice. We highlight the direction of the armchair and zigzag lines in red in the frame with $t = 0.8$ fs.

changing the value of $V^0_{pp\pi}$ and measuring the corresponding frequency f, we verified that the frequency is determined by $f = V^0_{pp\pi}/(2\pi\hbar) = 6.5 \times 10^{14}$ Hz. By introducing in the Hamiltonian higher-order hopping processes, the behavior of $C_i(t)$ becomes complex, and we cannot find a clear dominant frequency associated with any of the higher-order hopping terms. Fourier transforming $C_i(t)$ via Eq. (12) results in the local density of states, which shows the electron-hole symmetry in the NN and NNNN model, but not in the NNN model [36].

B. AA- and AB-stacking bilayer graphene

We will analyze in this section two particular cases of twisted bilayer graphene: AA and AB stacking. One should notice that we generate the TBG configurations by starting from the AA-stacking configuration and then twisting the two graphene layers about a vertical axis going through a pair of carbon atoms. Accordingly, the AA- and AB-stacking configurations are characterized by a twist angle of 0° and 60°, respectively. The point group symmetry of the AA- and AB-bilayer graphene is related to that of the monolayer.

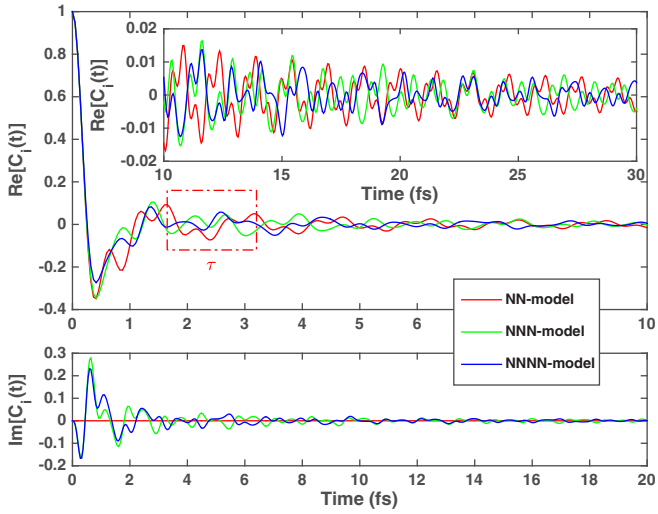

FIG. 2. The real and imaginary part of the autocorrelation function $C_i(t) = \langle i|\psi(t)\rangle$ calculated from three hopping models: the NN in red, the NNN in green, and the NNNN in blue. The red rectangle box identifies the typical oscillation pattern predicted by the NN model. The inset shows the continuous variation of the real part of $C_i(t)$ in a longer evolution time.

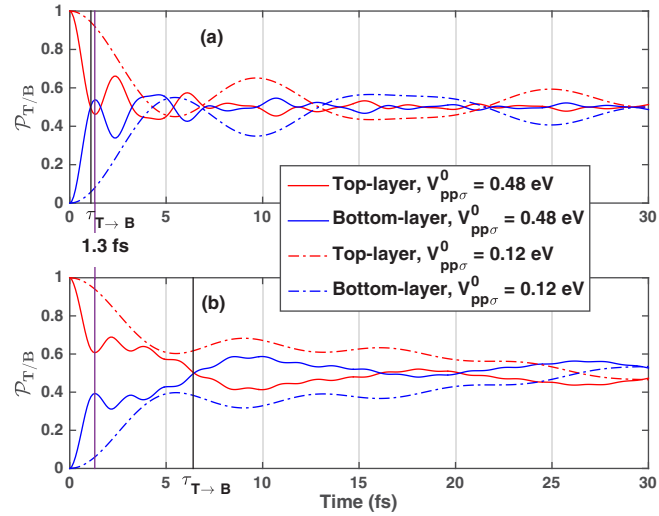

FIG. 3. Neutrino-like oscillation of the layer-integrated probability density $\mathcal{P}_{T/B}(t)$ for the (a) AA- and (b) AB-stacking bilayer graphene. Data plotted for two values of the Slater-Koster parameter $V^0_{pp\sigma} = 0.48$ eV (the solid curves) and 0.12 eV (the dot-dashed curves). Only data in the interval of (0, 30) fs are displayed to zoom in the oscillations. The vertical lines highlight the times $\tau_{T\to B}$ and $t = 1.3$ fs discussed in the text.

In other words, the symmetry of the AA-stacking bilayer graphene is characterized by the symmorphic space group $p6mm$, generated by the lattice translation and the point group D_{6h}, whereas the AB-stacking system is characterized by the symmorphic space group symmetry $P\bar{3}m1$ [41], generated by the lattice translation and the point group D_{3d} [42].

We start by considering the interlayer transfer of an electron wave function: we calculate the layer-integrated probability densities. This quantity is expressed as the summation of the probability density in each layer:

$$\mathcal{P}_\alpha(t) = \sum_{j\in(L_\alpha)} P_j(t)\ \forall\, \alpha \in \{\mathrm{T,B}\}. \tag{13}$$

In Fig. 3, we present the variation of $\mathcal{P}_\mathrm{T}$ and $\mathcal{P}_\mathrm{B}$ as a function of the time evolution. The layer-integrated probability density between the two graphene layers presents an oscillatory pattern as a function of time; this behavior is similar to the phenomenon discussed by Xian *et al.* as the neutrino-like oscillation [26]. In the case of the AA-stacking configuration, we observe how the wave on the top layer quickly penetrates into the bottom one compared to the AB-stacking configuration. After almost 1.3 fs, the transfer reaches a maximum of 54% before increasing yet again. We notice how different the oscillatory behaviors for the AA- and AB-stacking configurations are from each other, although the distance between the two graphene layers in the two systems $d = 3.35$ Å is the same. The hybridization of the $2p_z$ orbitals between the two graphene layers is also characterized by the same energy value of $V^0_{pp\sigma} = 0.48$ eV. To analyze the role of the interlayer coupling on the electron dynamics in the two-layer systems, we investigate the effects of tuning the interlayer coupling parameter $V^0_{pp\sigma}$ on the layer-integrated probability densities. In Fig. 3 we present these probabilities obtained by setting $V^0_{pp\sigma} = 0.48$ eV (the solid curves) and 0.12 eV (the dot-dashed curves). We observe how the reduction of $V^0_{pp\sigma}$ leads to an increase in the characteristic transfer time, which we define as the evolution time $\tau_{T\to B}$ needed to transfer 50% of the wave from the top layer to the bottom one. Calculation for various values of $V^0_{pp\sigma}$ shows that $\tau_{T\to B} \propto 1/V^0_{pp\sigma}$. At very long evolution time, each graphene layer supports about one-half of the initial waves, and the layer-interchange transfer becomes almost stationary with very weak oscillations in time. It is worthwhile to note that, for the AB-stacking configuration, we distinguished two cases of the initial state $|i\rangle$, one at the A-atom on top of the B-atom in the bottom layer, and the other at the B-atom on the center of the hexagonal ring underneath. We found that the layer-integrated probability densities in the two cases are the same, but the in-plane wave-spreading patterns are different, as discussed in next paragraphs. We now analyze the features of the intralayer spreading patterns in the AA- and AB-configurations. In Figs. 4 and 5 we present the evolution of a $2p_z$ state initially localized at a lattice node in the top layer of the two AA- and AB-stacking configurations of bilayer graphene, respectively. We use colors to represent the probability densities on two graphene layers, specifically red for the top layer and black for the bottom one. Similar to the case of monolayer graphene, the radius of the solid circle at each lattice node is proportional to the value of P_j normalized at the maximum value for each value of time.

By comparing the wavefront spreading behavior of the electron wave function in the monolayer graphene and that in the AA-stacking configuration for the evolution time $t <$ 1.3 fs, we realize that the distribution of $P_j(t)$ on the top and bottom graphene layers is similar to the case of monolayer graphene, but it becomes different for larger evolution time. It should be noticed from Fig. 3(a) that in the duration of (0, 1.3) fs, the top layer-integrated probability density $\mathcal{P}_\mathrm{T}$

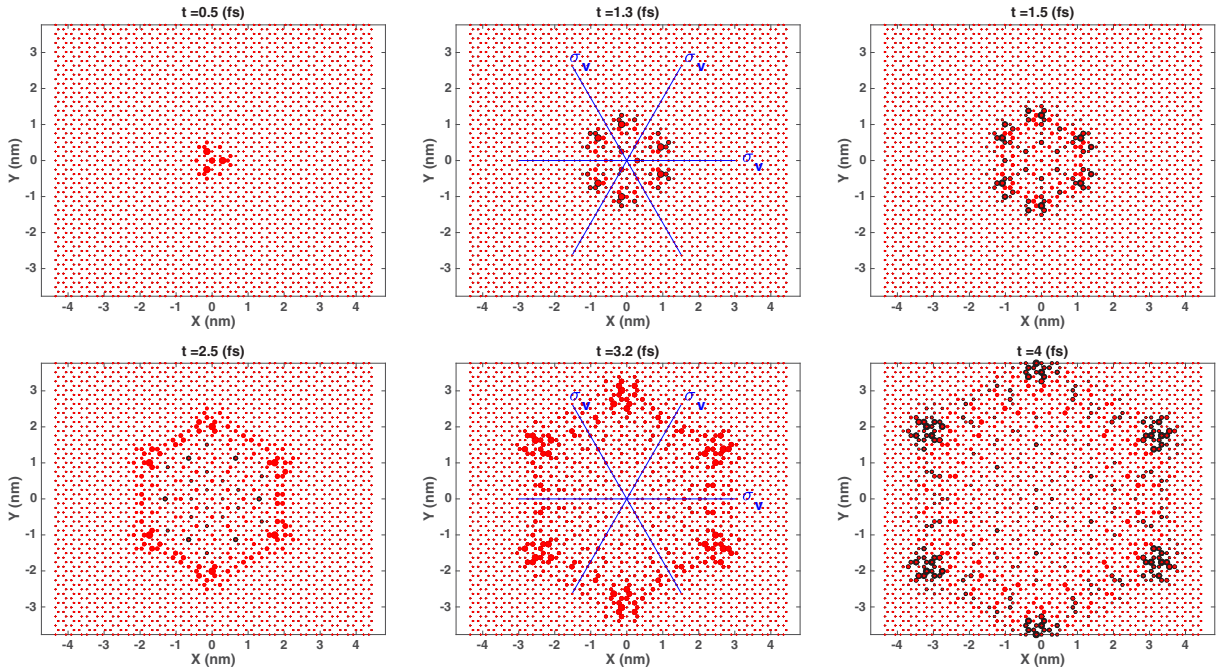

FIG. 4. Spreading of the electron probability density for the AA-stacking configuration taken at several time moments. Lattice nodes in red (black) belong to the top (bottom) graphene layer. The blue lines in the frames at $t = 1.3$ and 3.2 fs denote the three symmetrical mirrors σ_v of the lattice.

decreases monotonically. This means that the wave continues transferring to the bottom layer and achieves the maximal transferring percentage at 1.3 fs. When continuing to increase t, the part of the wave in the bottom layer transfers back to the top one. It results in the oscillation behavior of $\mathcal{P}_{\mathrm{T}}(t)$ and $\mathcal{P}_{\mathrm{B}}(t)$ similar to a Fabry-Pérot resonator. From Fig. 3(a) we can determine a set of characteristic time intervals, e.g., $(0, 1.3)$ fs, $(2.4, 4.6)$ fs, $(6.1, 7.3)$ fs, and so on, in which the wave transfers predominantly from the top to the bottom layer; alternatively, in the complementary time intervals the

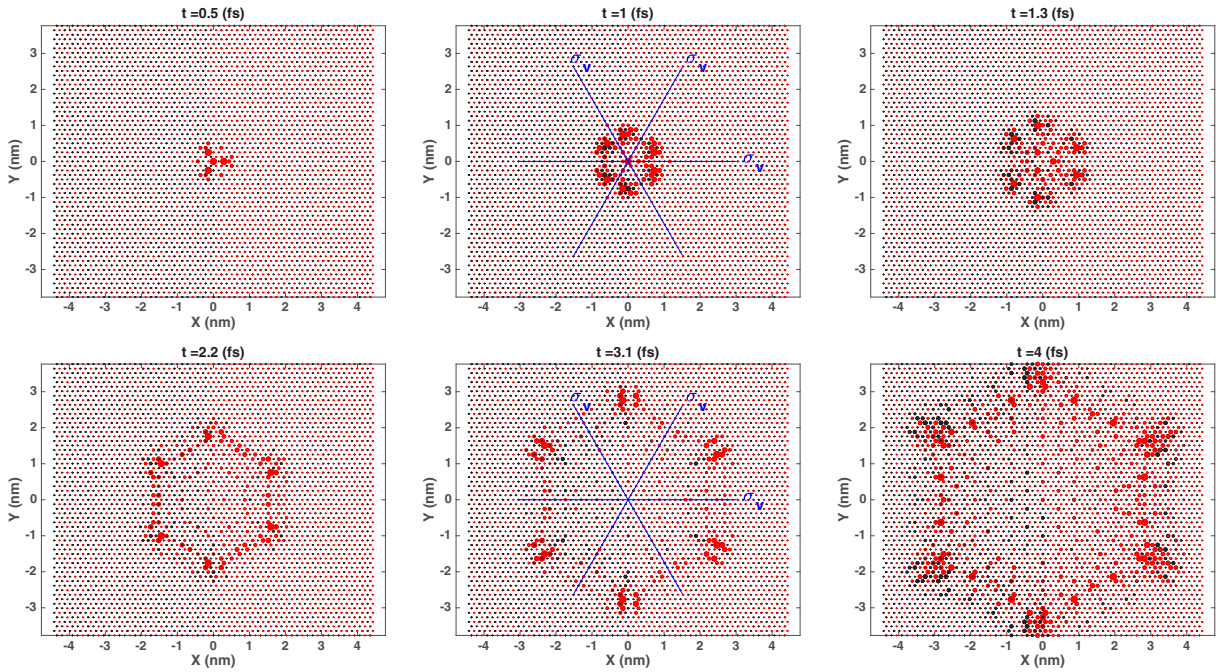

FIG. 5. Spreading of the electron probability density for the AB-stacking configuration taken at several time moments. The initial state $|i\rangle$ is set at the position of an A-atom of the top graphene layer, which is on top of a B-atom of the bottom layer. Lattice nodes in red (black) belong to the top (bottom) graphene layer. The blue lines in the frames at $t = 1$ and 3.1 fs denote the three symmetrical mirrors σ_v of the lattice.

wave transfers in the opposite direction. We found that after 1.3 fs, the distribution of $P_j(t)$ of monolayer graphene is not coincident to that on the top or the bottom layers of the bilayer system. This difference is a result of the combination of the intralayer and interlayer spreading induced by the hopping terms in the Hamiltonian (1). The wavefront at long evolution time presents a hexagonal shape similar to the monolayer graphene case. A direct inspection, however, shows that the form of the spreading pattern obeys only the point group C_{3v}. Remember that the symmetry of a node in the AA lattice is characterized by the point group D_{3h}, but the successive interlayer penetration of the electron wave lowers the symmetry of the distribution of probability densities to the C_{3v} symmetry.

For the AB-stacking configuration, we use the same technique for displaying data as for the AA configuration. From Fig. 3(b), we learn that for this configuration, the characteristic time $\tau_{\mathrm{T}\to\mathrm{B}} \approx 7$ fs is larger than for the AA one. We found that when $t < 1.3$ fs, the probability densities on the top layer are generally larger than those on the bottom one. The distribution of $P_j(t)$ on the top layer is identical to that of the monolayer graphene, but a quantitative difference becomes apparent when $t \in (1.3, 2.1)$ fs. When $t > 2.1$ fs, the probability densities on the bottom layer become comparable to those on the top layer and different from those on the monolayer graphene in both quantitative and qualitative aspects. Referencing Fig. 3(b), the interval $(0, 1.3)$ fs is the one in which the wave monotonically transfers from the top layer to the bottom one. Though the percentage of the wave transfer at $t \approx 1.3$ is smaller than 50%, successively the wave on the bottom layer transfers back to the top one. When this process occurs, it causes a change in the distribution of the probability densities from that of monolayer graphene. From Fig. 3(b) we determine the sets of time intervals $(0, 1.3)$ fs, $(2.2, 3.1)$ fs, $(3.9, 6.6)$ fs, and so on, in which the wave transfers predominantly from the top to the bottom layer, and in the complementary intervals where the wave transfers in the opposite direction. At long evolution time, the wave spreading is also characterized by a wavefront in the hexagonal shape that, similar to the AA-lattice case, reflects the plane symmetries of the lattice nodes in the AB-stacking system, i.e., the group C_{3v}, a subgroup of the point group D_{3d}.

We also calculated the time autocorrelation function $C_i(t)$ for the AA- and AB-stacking configurations. In Fig. 6 we present the data for $C_i(t)$ as a function of the time evolution for the two different parameter models: $V^0_{pp\sigma} = 0.48$ and 0.12 eV. We observe, in general, the intricate behavior of $C_i(t)$ in the two cases, which are different from each other. Interestingly, the figure shows the beating behavior of the autocorrelation functions when considering $V^0_{pp\sigma} = 0.12$ eV. Our calculation shows that the beating behavior does not appear clearly with $V^0_{pp\sigma} = 0.48$ eV, but it does when decreasing the value of $V^0_{pp\sigma}$ to the values smaller than about 0.3 eV. We also realize that the beating oscillation behavior is similar to the oscillation features of the time autocorrelation function of the monolayer graphene. It is expected because we should obtain a picture of the two independent graphene layers in the limit of $V^0_{pp\sigma} = 0$. This observation reflects the fact that the interlayer coupling plays the role of modulating the electronic states between the two graphene layers. When a wave is spreading in one layer, it penetrates partially into the other and thus creates

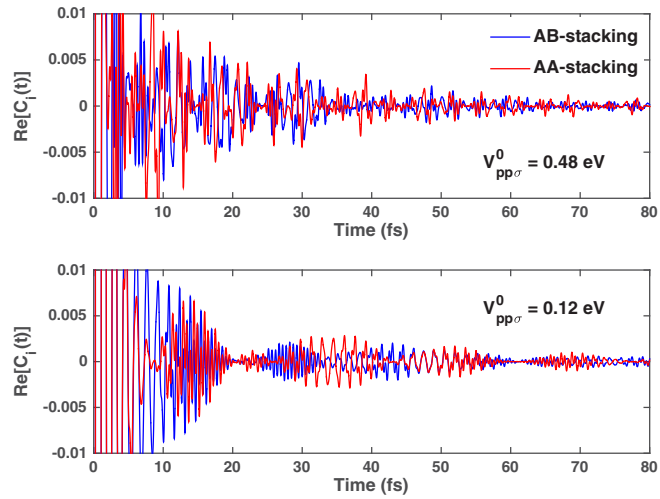

FIG. 6. Time autocorrelation functions $C_i(t)$ of the AA- (red) and AB-stacking (blue) bilayer graphene calculated using the NN model with $V^0_{pp\sigma} = 0.48$ and 0.12 eV.

two waves spreading in the two layers. The coupling between the two layers induces the exchange of wave between the two layers and forms the wave-interference pattern in the space limited by the two layers. The interference is sensitive to the alignment of the two atomic lattices. It thus explains the typical evolution features of electronic states in particular atomic configurations. Though the behavior of the autocorrelation functions versus the time is complicated, its Fourier transform results in the density of states of these two configurations [7,36].

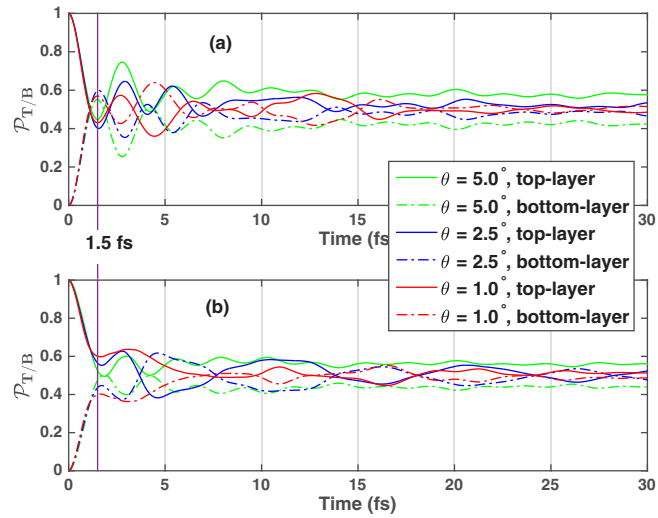

FIG. 7. Layer-integrated probability densities $\mathcal{P}_{\mathrm{T/B}}(t)$ in the top (solid lines) and bottom (dot-dashed lines) layers of three TBG configurations with the twist angles of 5° (green), 2.5° (blue), and 1° (red). Panels (a) and (b) are for the cases in which the initial state $|2p_z\rangle$ is located at the central point of the AA_0-like and AB-like region, respectively. The parameter $V_{pp\sigma} = 0.48$ eV. The vertical lines highlight the time $t = 1.5$ fs discussed in the text.

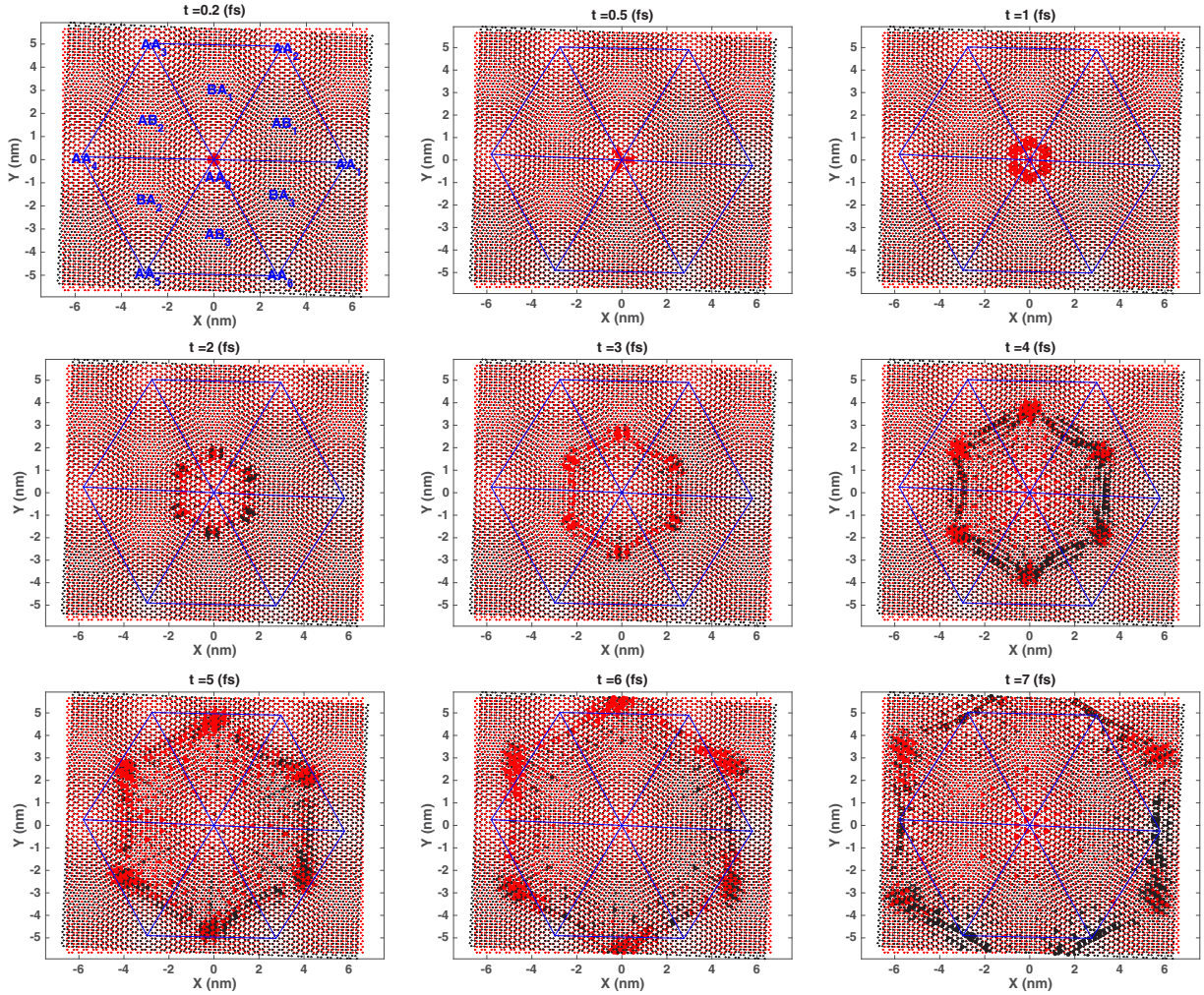

FIG. 8. Spreading of the electron probability density in the TBG configuration with $\theta = 2.5^\circ$ taken at several time moments. The initial state $|\psi(0)\rangle = |i\rangle$ located in the center of the AA-like region in the moiré zone. Lattice nodes in red (black) belong to the top (bottom) layer. The blue hexagon denotes the moiré zone. The characters AA_i ($i = 1, \ldots, 6$), AB_i, and BA_i ($i = 1, 2, 3$) remark the AA- and AB-like regions in the moiré zone.

C. Twisted bilayer graphene

Regarding the atomic structure, twisted bilayer graphene is a generalization of the AA- and AB-stacking bilayer systems with a generic rotation angle between the two graphene layers. In general, the alignment between the two graphene lattices in the TBG systems is not commensurate, i.e., not defined by a unit cell, and thus the lattice has very low symmetry. In the case of commensurate stacking, the space group characterizing the TBG lattice is determined to be either $p3m1$ or $p6mm$ depending on both the twist origin and the twist angles [11]. Interestingly, the generic TBG lattice shows a special moiré structure of the hexagonal form. In each moiré zone, we can find regions in which the atomic arrangement is close to the AA- and AB- or BA-stacking configurations. We illustrate the moiré zone in Fig. 8 with the blue hexagon where we marked the AA- and the AB-like regions [cf. the frame with $t = 0.2$ fs]. The AB-like regions are of two distinct types: one in which the A sublattice is in the top layer, and another in which the B sublattice is in the top layer. The AA-like and the two AB-like regions form two interpenetrating superlattices, a triangular and a honeycomb one, respectively. We investigated the electron time evolution in a series of TBG configurations with different twist angles. The qualitative behavior of the wave evolution is similar for the different twist angles we have investigated, thus we are going to present results for the case of two incommensurate twist angles 2.5° and 5°. The interlayer coupling always induces the wave transfer between the two graphene layers. Figure 7 shows that similar to the case of the AA-configuration, the transmission of the electron wave function from the top layer to the bottom one reaches a maximal value in about 1.5 fs. To illustrate the wave transfer between two graphene layers, we study the variation of the layer-integrated probability densities on time. Figure 7 shows the oscillation behavior of the layer-integrated probability densities for three incommensurate TBG configurations with a twist angle of 5° (green), 2.5° (blue), and 1° (red). (The last one is close to the first magic angle $\theta \approx 1.05^\circ$ [6].) Furthermore, we investigated how the layer-integrated probability densities change by changing the initial position: the panels (a) and (b) are for the cases in which the initial state is localized in the center of the AA_0-like and AB-like regions, respectively. We observe that the percentage of the

wave transmitted from the top layer to the bottom one depends on the twist angle. For a short time of evolution, $t < 5$ fs, the percentage is larger than 50% in the configuration with the twist angle of 5°. However, after 5 fs, there is about 60% of the wave propagating in the top layer and about 40% propagating in the bottom one. The minimal oscillation of the green curves $\mathcal{P}_{\mathrm{T/B}}(t)$ implies a very weak transfer of wave between the two layers. This dynamical observation supplements the explanation of the effective decoupling of the two graphene layers in the TBG configurations with large twist angles [6,43,44]. In other words, the two parts of the wave become nearly independently propagating on the two graphene layers after a long time evolution. For the TBG configurations with much smaller twist angles, e.g., 2.5° and 1°, after about 10 fs, the fluctuation of the blue and red curves $\mathcal{P}_{\mathrm{T/B}}(t)$ is always significant around the value of 50%. It implies a strong interaction between the two wave components when propagating in the TBG lattices with small twist angles.

We now present in Fig. 8 the intralayer spreading of a $2p_z$ state initially located at the central site of the AA-like region through the distribution of the probability densities $P_j(t)$. The time evolution is illustrated similarly to the case of the AA- and AB-stacking configurations. From the figure we observe that during the time interval (0, 2) fs, the initial state spreads similarly to case of the AA-stacking lattice, i.e., extending along the six preferable directions, and then a hexagonal wavefront is established. In this time interval, the wavefront takes the typical hexagonal shape, and it is still within the AA-like region. For time longer than $t = 3$ fs, we observe how the wavefront corners enter the AB-like regions, and the wavefront edges reach the transition regions between the AA_j and AA_0 regions. At this time, the probability densities start to be redistributed: they become concentrated in the AB-like regions as the six clusters seen in the time frame at $t = 4$ fs. These clusters then move in the transition regions between the AA_i and AA_{i+1} regions, i.e., along the zigzag lines connecting the AB-like regions in the first moiré zone to the other AB-like regions in the next moiré zones, while the probability densities on the edges of the hexagonal wavefront become scattered into the AA_{i+1} ($i \neq 0$) regions; see the time frames at $t = 5,\ 6$, and 7 fs. Though the wavefronts on the two graphene layers take the same hexagonal pattern, the distribution of the probability densities on those layers does not obey the hexagon symmetry group. By inspection, we observe that the symmetry of the wavefront reduces to the "approximate" C_3 symmetry. The wavefronts on the two graphene layers are not coincident due to the misalignment of the lattice stacking.

Interestingly, for long evolution time, we observe the higher intensity of the probability densities in the AA-like regions ($t > 15$ fs), particularly in the TBGs of tiny twist angles. This higher intensity is observed significantly in the AA_i region only; see Fig. 9. This observation might reflect the "localization" of low-energy Bloch wave functions in the AA-like regions as depicted in Refs. [6,7,18,19,36]. Notice that, at the evolution time t, we would expect the dominance of electron states of energies about $\hbar/t$. It therefore implies that, at long observation time, the localized signature shown in Fig. 9 of the electron wave function in the AA-like regions is the behavior of the states associated with the narrow energy band around the charge-neutrality level. This localization feature might also be related to topological properties of the wavefront as recently pointed out in Refs. [8,45,46]. Quantitatively, this association is consolidated by Fourier transforming the time autocorrelation $C(t)$ defined by Eq. (11) to obtain the density of states. The resulting DOS of the TBG configurations with the twist angles $\theta < 2.5°$ shows a small but significant peak around the charge-neutrality level as reported in Refs. [7,36].

In the following, once again, we will show how the dynamics of wave spreading in TBG strongly depends on the symmetry of an initially localized state. We now consider an initial $2p_z$ state at the central node of one AB-like region in the moiré zone. We note that, contrary to the central node in the AA-like regions, for this choice, there are no exact symmetry elements containing the central node of the AB-like regions. For short time evolution ($t < 1$ fs), the wave spreading is similar to that in the AB-stacking lattice. When increasing the evolution time, the wave evolves preferably in the directions heading three next-neighbor AB-like regions, i.e., along the zigzag lines separating the AA-like regions (cf. panel $t = 2$ fs

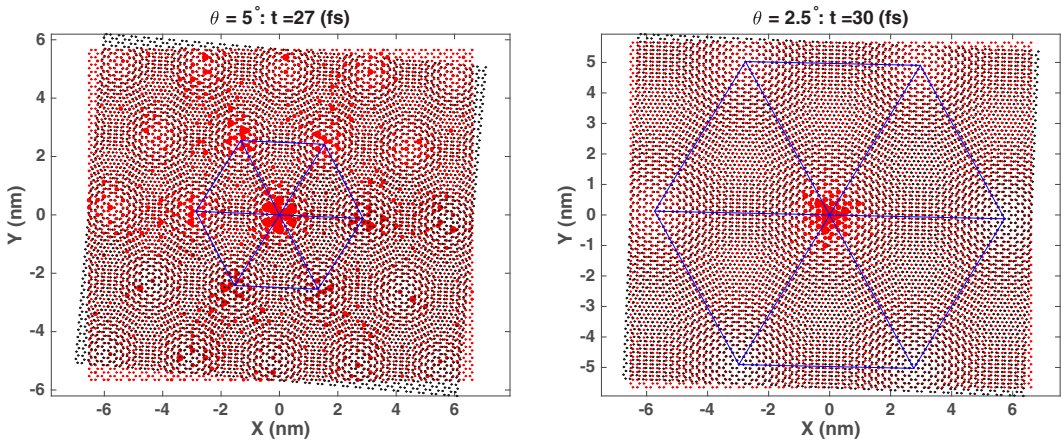

FIG. 9. Distribution of the probability densities in two TBG samples with $\theta = 5°$ (left panel) and $\theta = 2.5°$ (right panel) at large evolution times $t = 27$ and 30 fs.

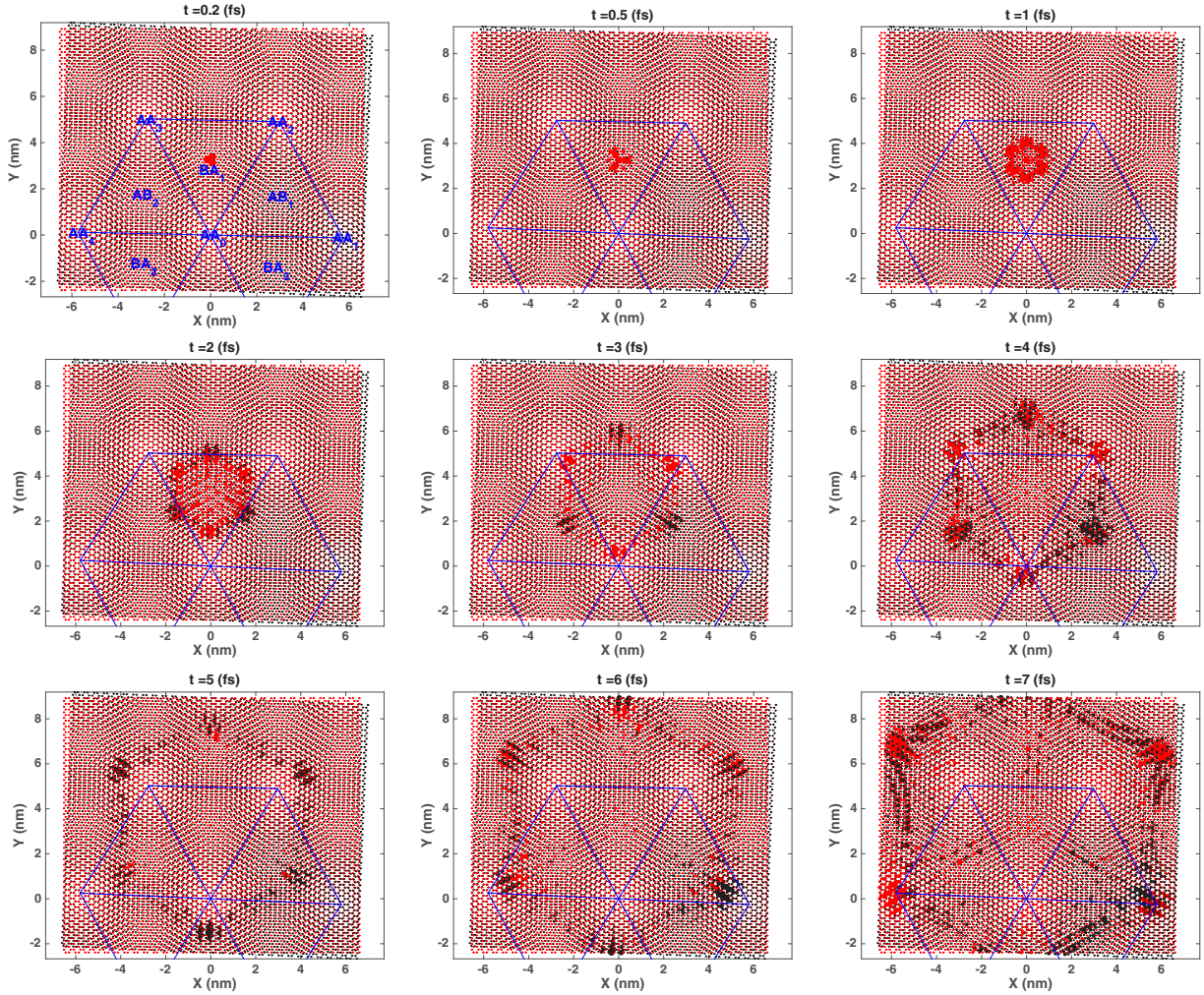

FIG. 10. Similar to Fig. 9 but with the initial state $|\psi(0)\rangle = |i\rangle$ located in the center of the AB-like region in the moiré zone. Lattice nodes in red (black) belong to the top (bottom) layer.

in Fig. 10). Along the opposite directions, the wave spreads into the AA-like regions, and the probability densities become concentrated at the center rather than scattered (cf. panels for $t = 3$ and 4 fs in Fig. 10). Following the distribution of the probability densities at larger times, the probability densities propagate along the zigzag lines in the transition regions between the AA_i- and AA_{i+1}-like regions and concentrated in the center of the AA-like regions. Due to the "approximated" symmetries about the initial position of the $2p_z$ state, the wavefront is formed and has an almost hexagonal shape. The six corners of the wavefront orient the preferably evolved directions. The distribution of $P_j(t)$ on the two layers satisfies the "approximated" point-group symmetry C_3.

To complete our discussion of the wave evolution in the TBG lattices, we present in Fig. 11 the time autocorrelation function $C(t)$. We remind the reader again that the choice of the initial condition has a crucial effect on the wave spreading. In Figs. 8 and 10, we have presented the data for two particular initial conditions, which result in typical spreading patterns of the $2p_z$ state. To extract quantitative information on observables, for instance the density of states, from the time evolution of electronic states we have to account

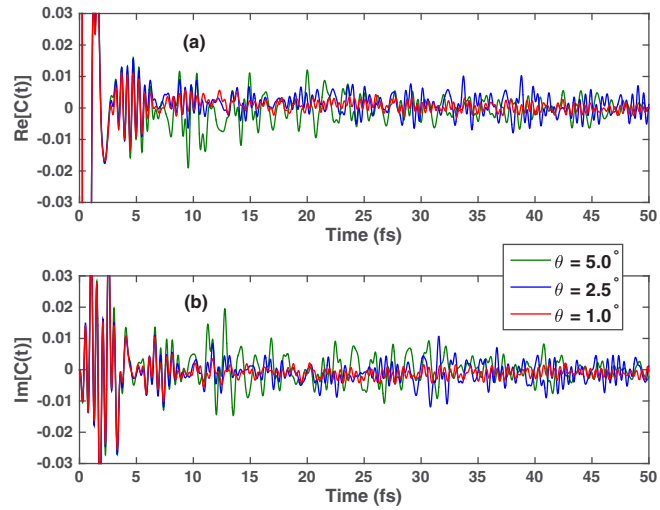

FIG. 11. The real (a) and imaginary (b) parts of the time autocorrelation function $C(t)$ for three TBG configurations with the twist angles of $\theta = 5^\circ$ (green), 2.5° (blue), and 1° (red).

for all possible initial conditions. According to Eq. (11), to calculate the time autocorrelation function $C(t)$, we need to calculate a set of functions $C_i(t) = \langle i|\psi(t)\rangle$ with the initial states $|i\rangle = |2p_z\rangle$ chosen at every lattice node in a sufficiently large TBG sample. Though a TBG lattice is not always defined by a unit cell with translational symmetry, the moiré zone can be seen as an approximated unit cell. It suggests that we need to consider only the lattice nodes in a moiré zone. However, since the typical length L_M defining the size of the moiré zone is related to the twist angle θ via the expression $L_M = \sqrt{3}a_{cc}/2\sin(\theta/2)$, it means that we have to work with a very large moiré for the TBG configurations in the case of a tiny twist angle—this can be a difficult task in practice. However, we demonstrated in Ref. [36] that an appropriate sampling scheme for a moderate number of lattice nodes in the moiré zone is sufficient to obtain reliable values for important physical observables. We apply here the same scheme to evaluate $C(t)$. The results are shown in Fig. 11 for three TBG configurations with $\theta = 5^\circ,\ 2.5^\circ$, and 1°. The figure shows the complex behavior of $C(t)$ as a function of time. Despite that, the Fourier transform of $C(t)$ [see Eq. (12)] results in the density of states with typical van Hove peaks shown in Refs. [7,36].

IV. CONCLUSION

We have presented a study of the time-evolution characteristics of electrons in bilayer graphene lattices with arbitrary twist angles. We used the Chebyshev polynomials of the first kind to approximate the time-evolution operator for a sufficiently long time evolution to calculate time-correlation functions reliably. We have shown that the interlayer electronic coupling induces the interchange transfer of waves between the two graphene layers, resulting in the oscillating behavior of the layer-integrated probability densities as a function of time, similar to complex Fabry-Pérot oscillations. This behavior can also be interpreted as the precession of electrons when describing the moiré-induced spatial modulation in the interlayer coupling in terms of non-Abelian gauge fields [47]. The percentage of the wave transmitted from one layer to the other depends on the twist angle, i.e., smaller than 50% and weak oscillation for large twist angles, $\theta > 2.5^\circ$, and larger than 50% and strong oscillation otherwise. This dynamical observation supplements the understanding of the effective decoupling between the two graphene layers in the TBG configurations with large twist angles. For the wave spreading in each graphene layer, we have indicated that the spreading shape of electron waves is dictated by the dominant hopping mechanism of the honeycomb pattern of the monolayer lattice and by the plane symmetries of the bilayer lattices. The wave spreading is irregular and takes place in two stages: The first one occurs within a very short time evolution, in which the wave spreads to the three nearest neighbors and then develops to the lattice nodes along the directions of the armchair lines of the honeycomb lattice. The second stage is characterized by the formation of a well-defined wavefront of hexagonal shape with the corners developing faster than the edges. For tiny twist TBG configurations, we have observed the signature of the electron localization in the AA-like regions inside the TBG's moiré zone at long time evolution. This would be associated with the formation of a narrow energy band around the charge-neutrality level. We have shown the interchange transfer of a wave between the two graphene layers resulting in the difference of the distribution of the probability densities on the TBG lattices from that on the monolayer. We have also observed the appearance of a beating pattern in the autocorrelation functions for a reduced intralayer coupling—it is possible to achieve this reduction experimentally [48]. This might suggest a way to engineer the electronic properties of bilayer systems. This study provides a complementary intuitive understanding of electron behavior in twisted bilayer graphene. The calculation method implemented here represents an alternative paradigm for future studies of exotic electronic properties of layered materials, including twisted bilayer graphene but also other van der Waals heterostructures.

ACKNOWLEDGMENTS

The work of V.N.D. and H.A.L. is supported by the National Foundation for Science and Technology Development (NAFOSTED) under Project No. 103.01-2016.62. The work of D.B. is supported by Spanish Ministerio de Ciencia, Innovation y Universidades (MICINN) under the project FIS2017-82804-P, and by the Transnational Common Laboratory *Quantum-ChemPhys*.

[1] M. Xu, T. Liang, M. Shi, and H. Chen, Graphene-like two-dimensional materials, Chem. Rev. **113**, 3766 (2013).

[2] A. K. Geim, and I. V. Grigorieva, Van der Waals heterostructures, Nature (London) **499**, 419 (2013).

[3] A. V. Rozhkov, A. O. Sboychakov, A. L. Rakhamanov, and F. Nori, Electronic properties of graphene-based bilayer systems, Phys. Rep. **648**, 1 (2016).

[4] J. M. B. Lopes dos Santos, N. M. R. Peres, and A. H. Castro Neto, Graphene Bilayer with a Twist: Electronic Structure, Phys. Rev. Lett. **99**, 256802 (2007).

[5] J. M. Lopes dos Santos, N. M. R. Peres, and A. H. Castro Neto, Continuum model of the twisted graphene bilayer, Phys. Rev. B **86**, 155449 (2012).

[6] R. Bistritzer and A. H. MacDonald, Moiré bands in twisted double-layer graphene, Proc. Natl. Acad. Sci. (USA) **108**, 12233 (2011).

[7] D. Weckbecker, S. Shallcross, M. Fleischmann, N. Ray, S. Sharma, and O. Pankratov, Low-energy theory for the graphene twist bilayer, Phys. Rev. B **93**, 035452 (2016).

[8] M. Koshino, N. F. Q. Yuan, T. Koretsune, M. Ochi, K. Kuroki, and L. Fu, Maximally Localized Wannier Orbitals and the Extended Hubbard, Phys. Rev. X **8**, 031087 (2018).

[9] Y. Cao, V. Fatemi, S. Fang, K. Watanabe, T. Taniguchi, E. Kaxiras, and P. Jarillo-Herrero, Unconventional superconductivity in magic-angle graphene superlattices, Nature (London) **556**, 43 (2018).

[10] Y. Cao, V. Fatemi, A. Demir, S. Fang, S. L. Tomarken, J. Y. Lou, J. D. Sanchez-Yamagishi, K. Watanable, T. Taniguchi, E. Kaxiras, R. C. Ashoori, and P. Jarillo-Herrero, Correlated insulator behavior at half-filling in magic-angle graphene superlattices, Nature (London) **556**, 80 (2018).

[11] L. Zou, H. C. Po, A. Vishwanath, and T. Senthil, Band structure of twisted bilayer graphene: Emergent symmetries, commensurate approximants, and Wannier obstructions, Phys. Rev. B **98**, 085435 (2018).

[12] M. Angeli, D. Mandelli, A. Valli, A. Amaricci, M. Capone, E. Tosatti, and M. Fabrizio, Emergent D_6 symmetry in fully relaxed magic-angle twisted bilayer graphene, Phys. Rev. B **98**, 235137 (2018).

[13] S. Shallcross, S. Sharma, and O. A. Pankratov, Quantum Interference at the Twist Boundary in Graphene, Phys. Rev. Lett. **101**, 056803 (2008).

[14] E. J. Mele, Interlayer coupling in rotationally faulted multilayer graphenes, J. Phys. D **45**, 154004 (2012).

[15] A. V. Rozhkov, A. O. Sboychakov, A. L. Rakhmanov, and F. Nori, Single-electron gap in the spectrum of twisted bilayer graphene, Phys. Rev. B **95**, 045119 (2017).

[16] J. C. Rode, D. Smirnov, C. Belke, H. Schmidt, and R. J. Haug, Twisted bilayer graphene: interlayer configuration and magnetotransport signatures, Ann. Phys. **529**, 1700025 (2017).

[17] E. S. Morell, J. D. Correa, P. Vargas, M. Pacheco, and Z. Barticevic, Flat bands in slightly twisted bilayer graphene, Phys. Rev. B **82**, 121407(R) (2010).

[18] G. Trambly de Laissardiere, D. Mayou, and L. Magaud, Localisation of Dirac electrons in rotated graphene bilayers, Nano Lett. **10**, 804 (2010).

[19] G. Trambly de Laissardiere, D. Mayou, and L. Magaud, Numerical studies of confined states in rotated bilayers of graphene, Phys. Rev. B **86**, 125413 (2012).

[20] K. Uchida, S. Furuya, J.-I. Iwata, and A. Oshiyama, Atomic corrugation and electron localization due to Moiré patterns in twisted bilayer graphenes, Phys. Rev. B **90**, 155451 (2014).

[21] P. Lucignano, D. Alfe, V. Cataudella, D. Ninno, and G. Cantele, The crucial role of atomic corrugation on the flat bands and energy gaps of twisted bilayer graphene at the "magic angle" $\theta \approx 1.08^\circ$, arXiv:1902.02690.

[22] W. Zawadzki and T. M. Rusin, Zitterbewegung (trembling motion) of electrons in semiconductors: A review, J. Phys.: Condens. Matter **23**, 143201 (2011).

[23] G. M. Maksimova, V. Ya. Demikhovskii, and E. V. Frolova, Wave packet dynamics in a monolayer graphene, Phys. Rev. B **78**, 235321 (2008).

[24] G. Márk, P. Vancsó, C. Hwang, P. Lambin, and L. P. Biró, Anisotropic dynamics of charge carriers in graphene, Phys. Rev. B **85**, 125443 (2012).

[25] A. Chaves, L. Covaci, Kh. Yu. Rakhimov, G. A. Farias, and F. M. Peeters, Wave-packet dynamics and valley filter in strained graphene, Phys. Rev. B **82**, 205430 (2010).

[26] L. Xian, Z. F. Wang, and M. Y. Chou, Coupled Dirac fermions and neutrino-like oscillation in twisted bilayer graphene, Nano Lett. **13**, 5159 (2013).

[27] A. H. Castro Neto, F. Guinea, N. M. R. Peres, K. S. Novoselov, and A. K. Geim, The electronic properties of graphene, Rev. Mod. Phys. **81**, 109 (2009).

[28] M. I. Katsnelson, Zitterbewegung, chirality, and minimal conductivity in graphene, Eur. Phys. J. B **51**, 157 (2006).

[29] E. Schrödinger, Über die kräftefreie bewegung in der relativistischen quantenmechanik, Sitzungsber. Preuss. Akad. Wiss. Phys. Math. Kl. **24**, 418 (1930).

[30] M. S. Jang, H. Kim, H. A. Atwater, and W. A. Goddard III, Time dependent behavior of a localised electron in a heterojunction boundary of graphene, Appl. Phys. Lett. **97**, 043504 (2010).

[31] V. Ya. Demikhovskii, G. M. Maksimova, A. A. Perov, and E. V. Frolova, Space-time evolution of Dirac wave packets, Phys. Rev. A **82**, 052115 (2010).

[32] Kh. Y. Rakhimov, A. Chaves, G. A. Farias, and F. M. Peeters, Wavepacket scattering of Dirac and Schrodinger particles on topical and magnetic barriers, J. Phys.: Condens. Matter **23**, 275801 (2011).

[33] S. T. Park, Propagation of a relativistic electron wave packet in the Dirac equation, Phys. Rev. A **86**, 062105 (2012).

[34] D. E. Fernandes, M. Rodrigues, and G. Falcao, Time evolution of electron waves in graphene superlattices, AIP Adv. **6**, 075109 (2016).

[35] A. Weibe, G. Wellein, A. Alvermann, and H. Fehske, The kernel polynomial method, Rev. Mod. Phys. **78**, 275 (2006).

[36] H. A. Le and V. N. Do, Electronic structure and optical properties of twisted bilayer graphene calculated via time evolution of states in real space, Phys. Rev. B **97**, 125136 (2018).

[37] P. Moon, and M. Koshino, Optical absorption in twisted bilayer graphene, Phys. Rev. B **87**, 205404 (2013).

[38] M. Koshino, Interlayer interaction in general incommensurate atomic layers, New. J. Phys. **17**, 015014 (2015).

[39] H. N. Nazareno, P. E. de Brito, and E. S. Rodrigues, Dynamics of wave packets in two-dimensional crystals under external magnetic and electric fields: formation of vortices, Phys. Rev. B **76**, 125405 (2007).

[40] E. Kogan, V. U. Nazarov, V. M. Silkin, and M. Kaveh, Energy bands in graphene: Comparison between the tight-binding model and *ab initio* calculations, Phys. Rev. B **89**, 165430 (2014).

[41] S. Latil and L. Henrard, Charge Carriers in Few-Layer Graphene Films, Phys. Rev. Lett. **97**, 036803 (2006).

[42] M. Koshino and E. McCann, Parity and valley degeneracy in multilayer graphene, Phys. Rev. B **81**, 115315 (2010).

[43] A. Luican, G. Li, A. Reina, J. Kong, R. R. Nair, K. S. Novoselov, A. K. Geim, and E. Y. Andrei, Single-Layer Behavior and its Breakdown in Twisted Graphene Layers, Phys. Rev. Lett. **106**, 126802 (2011).

[44] I. Brihuega, P. Mallet, H. González-Herrero, G. Trambly de Laissardière, M. M. Ugeda, L. Magaud, J. M. Gómez-Rodríguez, F. Ynduráin, and J.-Y. Veuillen, Unraveling the Intrinsic and Robust Nature of van Hove Singularities in Twisted Bilayer Graphene by Scanning Tunneling Microscopy and Theoretical Analysis, Phys. Rev. Lett. **109**, 196802 (2012).

[45] H. Ch. Po, L. Zou, A. Vishwanath, and T. Senthil, Origin of Mott Insulating Behavior and Superconductivity in Twisted Bilayer Graphene, Phys. Rev. X **8**, 031089 (2018).

[46] J. Kang and O. Vafek, Symmetry, Maximally Localized Wannier States, and a Low-Energy Model for Twisted Bilayer Graphene Narrow Bands, Phys. Rev. X **8**, 031088 (2018).

[47] P. San Jose, J. González, and F. Guinea, Non-Abelian Gauge Potentials in Graphene Bilayers, Phys. Rev. Lett. **108**, 216802 (2012).

[48] J. W. Jeon, H. Kim, H. Kim, S. Choi, and B. H. Kim, Experimental evidence for interlayer decoupling distance of twisted bilayer graphene, AIP Adv. **8**, 075228 (2018).